Saliency Extraction and Torque Sharing Estimation of Dual Motor Drive using Special Current Sensor Configuration

E. Rodriguez Montero[1], M. Vogelsberger[2], T. Wolbank[1]
TU WIEN[1]
Gusshausstrasse 27/29 E370-2, 1040
Vienna, Austria.
Tel.: +43 (1) 58801 – 370226[1]
thomas.wolbank@tuwien.ac.at[1]
ALSTOM TRANSPORT AUSTRIA GMBH[2]
Rolling Stock & Components
Bogies & DRIVES – Product Family
Hermann Gebauer Straße 5, 1220
Vienna, Austria.
Tel.: +43 (1) 25110 – 599[2]
markus.vogelsberger@alstomgroup.com[2]

Acknowledgements

The authors want to thank ALSTOM, especially Mr. H. Mannsbarth (head of Components-Bogies/Drives department in global Rolling Stock Platform/Components division) and Mr. Cedric Zanutti (head of R&D/Technology in RSC-Bogies/Drives), for their generous support, research/development funding and project supervision. Furthermore, the authors want to thank colleagues from ALSTOM group (Mr. Newesely, Mr. Cepak, Mr. Harasleben, Mr. Ganster and Mr. E. Moser), as well as Prof. Dr. H. Ertl (TU-Wien) for all their feedback and great support.

The authors are very indebted to LEM Company (especially Mr. A. Hürlimann/Chairman of Board of Directors, Dr. W. Teppan & Mr. J. Burk) for cooperation and generous support.

Keywords

«Current sensor», «Induction motors», «Parallel operation», «Sensorless control», «Signal processing»

Abstract

Dual motor drives refer to the control of two motors connected in parallel and fed by a single inverter. This type of drives is usual in some industry fields such as railway applications or conveyor drives. The control performance as well as the feasibility for saliency extraction are highly impacted by the arrangement and amount of current sensors equipped in the drive. Commonly, four current sensors in total are attached to two phases of each motor, thus permitting torque sharing calculation and individual spatial saliency extraction.

In this work, two different current sensor configurations are applied to an experimental test stand consisting of two induction motors connected in parallel and fed by a single inverter. The two current sensor configurations are investigated and discussed for encoderless saliency extraction, control performance and torque sharing estimation capability.

Introduction

Voltage step excitation methods [1-4] are a robust way to extract motor saliencies. Using the rotor information that saliencies contain, these methods permit encoderless speed control. They are based on the estimation of the transient leakage inductance, since, within it, motor saliencies are present.

According to the stator voltage equation, the resulting time current derivative relates to the transient leakage inductance after the inverter performs a voltage step. Yet, it also relates to the back EMF (electro-motive force) and stator resistance. Therefore, signal processing is required.

The vector combination of certain phase current slopes resulting from specific voltage steps leads to a saliency-offset vector, composed of an offset and a saliency-modulated term. In multiple ways, signal offset can be compensated. Preferably, offset can be accurately estimated using specific vector combinations [3]. In case it is mathematically not feasible, feedforward compensation can be done [1]. In the field of dual motors, voltage step excitation was applied in [1]. A current sensor configuration was proposed, where two current sensors were attached to the first motor (M1), and one to the second motor (M2). Using specific voltage step excitations and signal processing, a saliency vector was obtained for each motor separately. While M1 saliency vector achieved offset elimination by vector combinations of phase current slopes, M2 offset was eliminated via feedforward compensation. In addition, in [2] load sharing calculation was possible using a M2 stator current phasor estimator. According to literature [5-7], awareness of load sharing knowledge can improve performance.

In this work, two different current sensor configurations are applied to an experimental test stand consisting of two induction motors connected in parallel and fed by a single inverter. The two configurations are investigated and discussed for encoderless saliency extraction, control performance and torque sharing estimation capability. A FOC (field-oriented control) strategy is proposed, based on a single torque and flux estimator is implemented. The torque and flux estimator receives the average rotor angle and the average stator current as input.

In the first current sensor configuration (conf1), two current sensors are attached to two inverter output phases, thus measuring sum current of both machines. A third sensor is attached to an arbitrary motor phase (e.g. phase C M2). It will be shown that, using this configuration, both M1 and M2 require feedforward offset compensation in order to access motor saliencies. Besides, load sharing calculation is possible using a stator current estimator for each motor.

In the second current sensor configuration (conf2), two current sensors are attached to the A and B phases of M1. A third sensor is attached to M2 phase C. As it will be shown, conf2 allows for acquisition of an offset-less saliency vector for M1. However, for M2, a saliency-offset vector is obtained, thus requiring elimination. Besides, load sharing calculation is possible using a single stator current estimator for motor M2, at which only one current sensor is attached. Because the average stator current is not measured but estimated, performance might decrease.

Experimental results prove the functionality of both current sensor configurations for encoderless vector control and torque-sharing calculation, and discuss the benefits and drawbacks of each current sensor configuration.

Current sensor configurations

For vector control of two parallel motors, a standard practice is to measure the stator current vector of each motor by attaching two current sensors at each motor [5-10]. An advantage of this current sensor configuration is that the torque and flux of each motor can be calculated individually. Awareness of torque sharing can improve drive operation in terms of stability and performance [5-7].
As mentioned before, this paper proposes using only three current sensors, arranged in two different ways and compares them regarding saliency extraction, vector control and load-sharing estimation capability. For the analysis, three-phase balanced currents are assumed.

Both current sensor configurations are shown in Fig. 1. As observed, sum stator current vector is measured in conf1, together with phase C current of M2. In contrast, in conf2, stator current vector of M1 together with phase C current of M2.

In Fig. 1, M1 and M2 are represented by their transient leakage inductance L, back EMF E, and stator resistance R_S. ABC denote the three motor phases, and N an arbitrary phase. Within the inverter, SVPWM (space vector pulse width modulation) inverter output states are depicted.

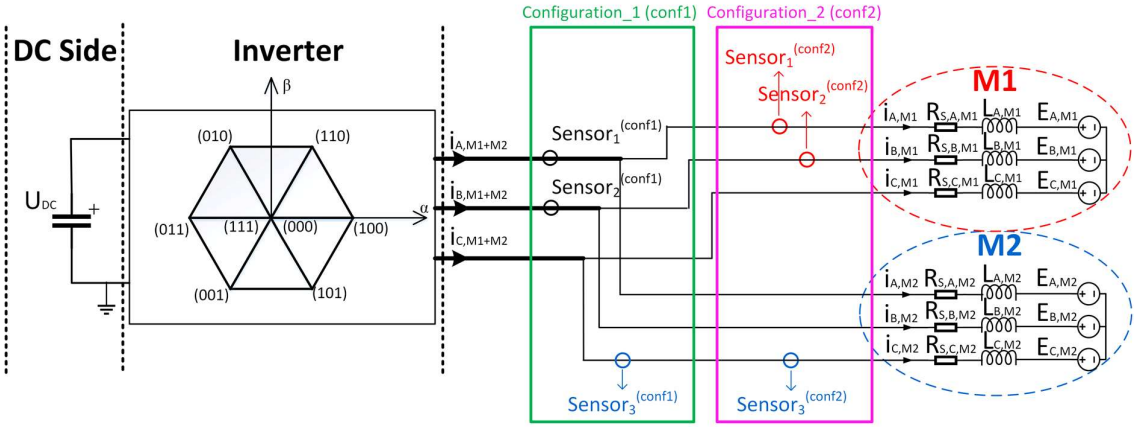

Fig. 1: Schematic representation of the DC-link, inverter and dual motors. The two current sensor configurations are shown (conf1 and conf2).

Saliency extraction using voltage step excitation

Voltage step excitation methods [1-4] rely on the extraction of the machine saliencies observed at the leakage inductance. The leakage inductance is visible in the phase current response that results from inverter active switching. According to the M1 and M2 models of Fig. 1, (1)-(3) hold true:

$$U_{AB} = R_{S,A} \cdot i_A + L_A \cdot di_A/dt + E_A - (R_{S,B} \cdot i_B + L_B \cdot di_B/dt + E_B) \quad (1)$$

$$U_{CA} = R_{S,C} \cdot i_C + L_C \cdot di_C/dt + E_C - (R_{S,A} \cdot i_A + L_A \cdot di_A/dt + E_A) \quad (2)$$

$$U_{BC} = R_{S,B} \cdot i_B + L_B \cdot di_B/dt + E_B - (R_{S,C} \cdot i_C + L_C \cdot di_C/dt + E_C) \quad (3)$$

As observed in (1-3), the phase current slopes after inverter switching transition are linked to the transient leakage inductances L_A, L_B, L_C. Moreover, U_{AB}, U_{AC}, U_{BC} vary according to Table I depending on the switching state.

Table I: Inverter output voltages for 2-level 3-phase inverter

	100	110	010	011	001	101	000&111
U_{AB}	U_{DC}	0	$-U_{DC}$	$-U_{DC}$	0	U_{DC}	0
U_{BC}	0	U_{DC}	U_{DC}	0	$-U_{DC}$	$-U_{DC}$	0
U_{CA}	$-U_{DC}$	$-U_{DC}$	0	U_{DC}	U_{DC}	0	0

Due to the presence of saliencies in the induction motor, the transient leakage can be expressed as:

$$L_A = L_0 + L_m \cdot sin(2 \cdot \pi \cdot f_{sal} \cdot t) \quad (4)$$

$$L_B = L_0 + L_m \cdot sin(2 \cdot \pi \cdot f_{sal} \cdot t + 2 \cdot \pi/3) \quad (5)$$

$$L_C = L_0 + L_m \cdot sin(2 \cdot \pi \cdot f_{sal} \cdot t + 4 \cdot \pi/3) \quad (6)$$

Where L_0 denotes symmetrical transient inductance or transient inductance offset, and $L_m \cdot sin(2 \cdot \pi \cdot f_{sal} \cdot t)$ the modulation of the transient inductance due to one saliency that revolves with f_{sal} frequency and L_m amplitude.

Saliency extraction for conf1

The extraction of the saliencies of M1 and M2 for conf1 is explained in this subsection. The excitation sequence chosen in this work is the three sets of antiparallel inverter states (100&011, 010&101 and 001&110). The resulting phase current slopes, depending on the current sensor configuration, are combined to form a saliency-offset vector and are further processed to extract rotor-slotting saliency.

For M1, the calculated current slopes are vector combined as in (7) for the 100-011 excitation sequence. Applying Kirchhoff's law, M1 phase C current can be obtained as in (8).

$$\Delta i_{M1,100}^{(conf1)} - \Delta i_{M1,011}^{(conf1)} = \left(\frac{di_{C,M1,100}^{(conf1)}}{dt} - \frac{di_{C,M1,011}^{(conf1)}}{dt}\right) \tag{7}$$

$$\frac{di_{C,M1,100}^{(conf1)}}{dt} - \frac{di_{C,M1,011}^{(conf1)}}{dt} = \\ = -\left(\frac{di_{A,M1+M2,100}^{(conf1)}}{dt} - \frac{di_{A,M1+M2,011}^{(conf1)}}{dt}\right) - \left(\frac{di_{B,M1+M2,100}^{(conf1)}}{dt} - \frac{di_{B,M1+M2,011}^{(conf1)}}{dt}\right) - \left(\frac{di_{C,M2,100}^{(conf1)}}{dt} - \frac{di_{C,M2,011}^{(conf1)}}{dt}\right) \tag{8}$$

For M2, (9) is applied.

$$\Delta i_{M2,100}^{(\mathrm{conf1})} - \Delta i_{M2,011}^{(\mathrm{conf1})} = \left(\frac{di_{C,M2,100}^{(conf1)}}{dt} - \frac{di_{C,M2,011}^{(conf1)}}{dt}\right) \tag{9}$$

After computing (7-9) for the other sets of excitation sequence, the saliency-offset vectors for M1 and M2 are formed using (10) and (11).

$$\bar{v}_{sal,M1}^{(conf1)} = (\Delta i_{M1,100}^{(\mathrm{conf1})} - \Delta i_{M1,011}^{(\mathrm{conf1})}) \cdot e^{i\cdot 5\cdot\frac{\pi}{3}} + \left(\Delta i_{M1,010}^{(\mathrm{conf1})} - \Delta i_{M1,101}^{(\mathrm{conf1})}\right) \cdot e^{i\cdot 9\cdot\frac{\pi}{3}} + \left(\Delta i_{M1,001}^{(\mathrm{conf1})} - \Delta i_{M1,110}^{(\mathrm{conf1})}\right) \cdot e^{i\cdot\frac{\pi}{3}} \tag{10}$$

$$\bar{v}_{sal,M2}^{(conf1)} = (\Delta i_{M2,100}^{(\mathrm{conf1})} - \Delta i_{M2,011}^{(\mathrm{conf1})}) \cdot e^{i\cdot 5\cdot\frac{\pi}{3}} + \left(\Delta i_{M2,010}^{(\mathrm{conf1})} - \Delta i_{M2,101}^{(\mathrm{conf1})}\right) \cdot e^{i\cdot 9\cdot\frac{\pi}{3}} + \left(\Delta i_{M2,001}^{(\mathrm{conf1})} - \Delta i_{M2,110}^{(\mathrm{conf1})}\right) \cdot e^{i\cdot\frac{\pi}{3}} \tag{11}$$

The result of (10) and (11) is a saliency-offset vector for both M1 and M2 as shown in (12) and (13), with $L_{0,M2} \cdot e^{i\left(\frac{\pi}{6}\right)}$ as offset and $\frac{1}{2} \cdot L_{m,M2} \cdot e^{i\cdot(2\cdot\pi\cdot f_{sal,M2}\cdot t)}$ as saliency-modulated term.

$$\bar{v}_{sal,M1}^{(conf1)} = (L_{0,M2} \cdot e^{i\left(\frac{\pi}{6}\right)} - \frac{1}{2} \cdot L_{m,M2} \cdot e^{i\cdot(2\cdot\pi\cdot f_{sal,M2}\cdot t)}) \cdot cst_{M1} \tag{12}$$

$$\bar{v}_{sal,M2}^{(conf1)} = (L_{0,M2} \cdot e^{i\left(\frac{\pi}{6}\right)} - \frac{1}{2} \cdot L_{m,M2} \cdot e^{i\cdot(2\cdot\pi\cdot f_{sal,M2}\cdot t)}) \cdot cst_{M2} \tag{13}$$

Where cst is constant at constant torque and constant DC voltage.

$$cst_{M1} = U_{DC} \cdot \left(L_{0,M1}^2 - 1/4 \cdot L_{m,M1}^2\right)^{-1} \tag{14}$$

$$cst_{M2} = U_{DC} \cdot \left(L_{0,M2}^2 - 1/4 \cdot L_{m,M2}^2\right)^{-1} \tag{15}$$

Saliency extraction for conf2

The extraction of the saliencies of M1 and M2 for conf2 is explained in this subsection.

The calculated M1 current slopes, using the available current sensors, are vector combined as in (16-17) for the 100-011 excitation sequence.

$$\Delta i_{M1,100}^{(\mathrm{conf2})} - \Delta i_{M1,011}^{(\mathrm{conf2})} = \\ = \frac{di_{A,M1,100}^{(conf\ )}}{dt} - \frac{di_{A,M1,011}^{(conf2)}}{dt} + \left(\frac{di_{B,M1,100}^{(conf2)}}{dt} - \frac{di_{B,M1,011}^{(conf2)}}{dt}\right) \cdot e^{i\left(2\cdot\frac{\pi}{3}\right)} + \left(\frac{di_{C,M1,100}^{(co\ )}}{dt} - \frac{di_{C,M1,011}^{(conf\ )}}{dt}\right) \cdot e^{i\left(4\cdot\frac{\pi}{3}\right)} \tag{16}$$

$$\frac{di_{C,M1,100}^{(conf2)}}{dt} - \frac{di_{C,M1,011}^{(conf2)}}{dt} = -\left(\frac{di_{A,M1,100}^{(conf2)}}{dt} - \frac{di_{A,M1,011}^{(conf2)}}{dt}\right) - \left(\frac{di_{B,M1,100}^{(conf2)}}{dt} - \frac{di_{B,M1,011}^{(conf2)}}{dt}\right) \quad (17)$$

For M2, (18) is applied.

$$\Delta i_{M2,100}^{(\text{conf2})} - \Delta i_{M2,011}^{(\text{conf2})} = \left(\frac{di_{C,M2,100}^{(conf2)}}{dt} - \frac{di_{C,M2,011}^{(conf2)}}{dt}\right) \quad (18)$$

After computing (16-18) for the other sets of excitations, the saliency-offset vectors for M1 and M2 are formed using (19) and (20).

$$\bar{v}_{sal,M1}^{(conf2)} = \Delta i_{M1,100}^{(\text{conf2})} - \Delta i_{M1,011}^{(\text{conf2})} + \left(\Delta i_{M1,010}^{(\text{conf2})} - \Delta i_{M1,101}^{(\text{conf2})}\right) \cdot e^{i \cdot 2 \cdot \frac{\pi}{3}} + \left(\Delta i_{M1,001}^{(\text{conf2})} - \Delta i_{M1,110}^{(\text{conf2})}\right) \cdot e^{i \cdot 4 \cdot \frac{\pi}{3}} \quad (19)$$

$$\bar{v}_{sal,M2}^{(conf2)} = (\Delta i_{M2,100}^{(\text{conf2})} - \Delta i_{M2,011}^{(\text{conf2})}) \cdot e^{i \cdot 5 \cdot \frac{\pi}{3}} + \left(\Delta i_{M2,010}^{(\text{conf2})} - \Delta i_{M2,101}^{(\text{conf2})}\right) \cdot e^{i \cdot 9 \cdot \frac{\pi}{3}} + \left(\Delta i_{M2,001}^{(\text{conf2})} - \Delta i_{M2,110}^{(\text{conf2})}\right) \cdot e^{i \frac{\pi}{3}} \quad (20)$$

The result of (19) and (20) is a saliency vector for M1 as shown in (21) and a saliency-offset vector for M2 as shown in (22).

$$\bar{v}_{sal,M1}^{(conf2)} = -3/2 \cdot L_{m,M1} \cdot e^{i \cdot (2 \cdot \pi \cdot f_{sal,M1} \cdot t)} \cdot cst_{M1} \quad (21)$$

$$\bar{v}_{sal,M2}^{(conf2)} = (L_{0,M2} \cdot e^{i\left(\frac{\pi}{6}\right)} - \frac{1}{2} \cdot L_{m,M2} \cdot e^{i \cdot (2 \cdot \pi \cdot f_{sal,M2} \cdot t)}) \cdot cst_{M2} \quad (22)$$

Stator current vector estimation

According to literature, awareness on the torque sharing can improve dual motor drive performance [5-7]. In order to compute torque sharing, the stator current as well as rotor position of M1 and M2 must be available. Rotor angle is in this work calculated from the slotting saliency as explained in previous section. When it comes to stator current phasor, it is proposed to calculate M1 current phasor $\bar{\imath}_{S,M1}$ using Sensor1(conf2) and Sensor2(conf2), and estimate M2 current phasor $\bar{\imath}_{S,M2}$using signal processing, summarized in (23-26).

$$\bar{\imath}_{S,M1}^{(conf2)} = i_{A,M1}^{(conf2)} + i_{B,M1}^{(conf2)} \cdot a + (-i_{A,M1}^{(conf2)} - i_{B,M1}^{(conf2)}) \cdot a^2 \quad (23)$$

Phase C currents of M1 and M2 are represented as in (24), with I_C amplitude and δ_C phase shift.

$$i_C = I_C \cdot \sin(w_e \cdot t + \delta_C) \quad (24)$$

Since both motors have the same electrical frequency, $\bar{\imath}_{S,M2}$ can be estimated using (25-26).

$$\bar{k}_{M2}^{(conf2)} = \frac{I_{C,M2} \cdot e^{j \cdot \delta_{C,M2}}}{I_{C,M1} \cdot e^{j \cdot \delta_{C,M1}}} = \frac{I_{C,M2}}{I_{C,M1}} \cdot e^{j \cdot (\delta_{C,M2} - \delta_{C,M1})} \quad (25)$$

$$\bar{\imath}_{S,M2}^{(conf2)} = \bar{\imath}_{S,M1}^{(conf2)} \cdot \bar{k}_{M2}^{(conf2)} \quad (26)$$

Where the amplitude division and phase shift difference of (25) is computed using FFT over a half electrical period.

Regarding conf1, the sum current phasor $\bar{\imath}_{S,M1+M2}^{(conf1)}$ is computable as in (27). Since the electrical frequency is equal for M1 and M2, $\bar{\imath}_{S,M1}^{(conf1)}$ and $\bar{\imath}_{S,M2}^{(conf1)}$ can be estimated using (28-31).

$$\bar{\imath}_{S,M1+M2}^{(conf1)} = i_{A,M1+M2}^{(conf1)} + i_{B,M1+M2}^{(conf1)} \cdot a + (-i_{A,M1+M2}^{(conf1)} - i_{B,M2}^{(conf1)}) \cdot a^2 \quad (27)$$

$$\bar{k}_{M1}^{(conf1)} = \frac{I_{C,M1} \cdot e^{j \cdot \delta_{C,M1}}}{I_{C,M1+M2} \cdot e^{j \cdot \delta_{C,M1+M2}}} = \frac{I_{C,M1}}{I_{C,M1+M2}} \cdot e^{j \cdot (\delta_{C,M1} - \delta_{C,M1+M2})} \quad (28)$$

$$\bar{\imath}_{S,M1}^{(conf1)} = \bar{\imath}_{S,M1+M2}^{(conf1)} \cdot \bar{k}_{M1}^{(conf1)} \tag{29}$$

$$\bar{k}_{M2}^{(conf1)} = \frac{I_{C,M2} \cdot e^{j\cdot\delta_{C,M2}}}{I_{C,M1+M2} \cdot e^{j\cdot\delta_{C,M1+M2}}} = \frac{I_{C,M2}}{I_{C,M1+M2}} \cdot e^{j\cdot(\delta_{C,M2}-\delta_{C,M1+M2})} \tag{30}$$

$$\bar{\imath}_{S,M2}^{(conf1)} = \bar{\imath}_{S,M1+M2}^{(conf1)} \cdot \bar{k}_{M2}^{(conf1)} \tag{31}$$

Where the amplitude divisions and phase shift differences of (28) and (30) are computed using FFT over a half electrical period.

Control strategy

This section shows and compares the control scheme used for conf1 and conf2. The control strategy used for both configurations in this work is based on average FOC using a single flux and torque estimator. The input to the average FOC scheme is the average stator current phasor, and the average rotor angle. Note that, for conf1, average stator current is available given the sensor arrangement, while for conf2, average stator current must be calculated using (27) and (31). The block diagram of the control scheme for conf1 and conf2 are shown in Fig. 2 and Fig. 3, respectively.

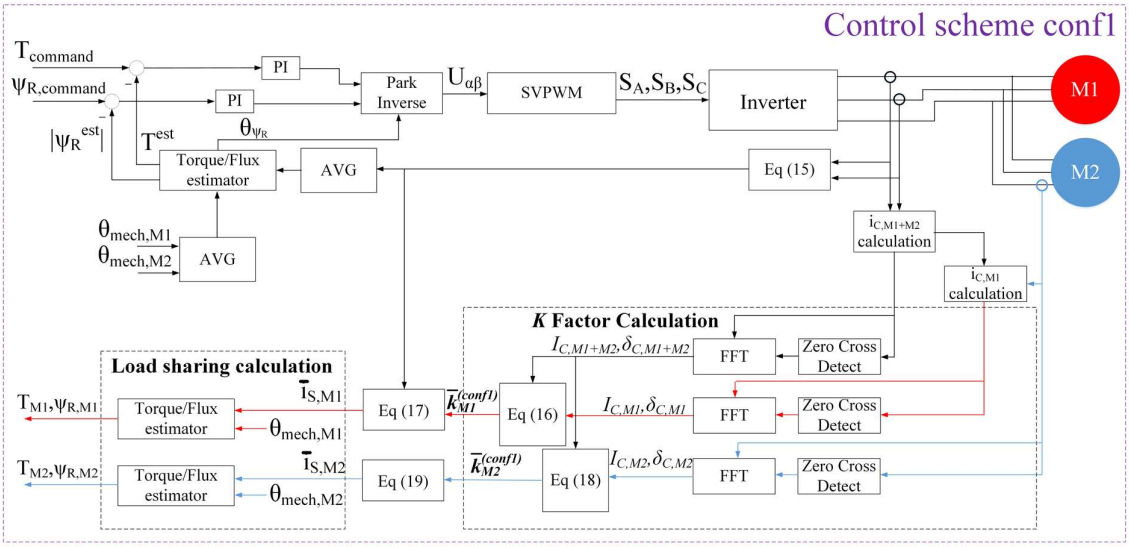

Fig. 2: control scheme for conf1.

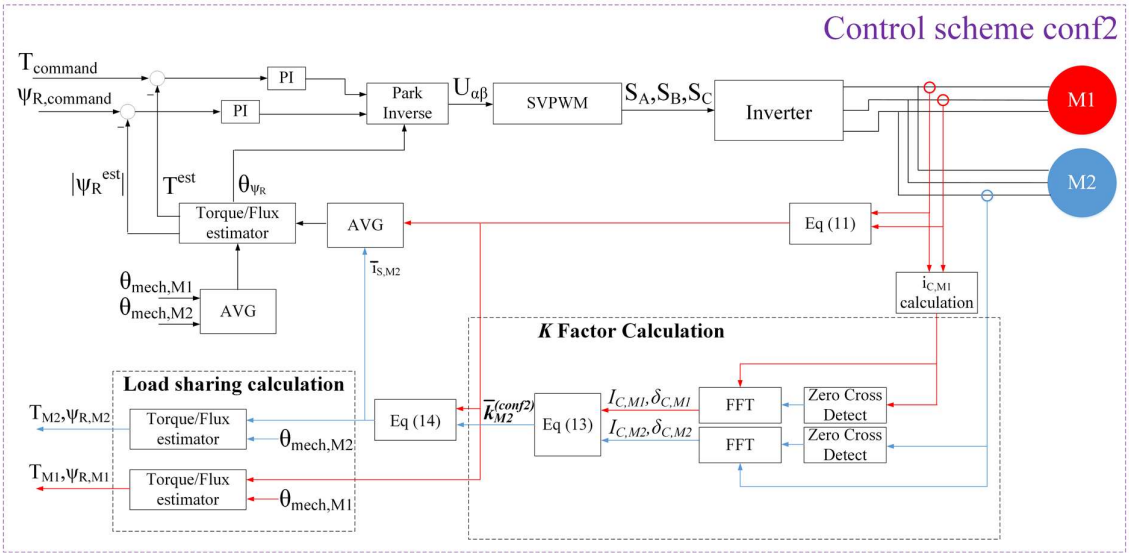

Fig. 3: control scheme for conf2.

Experimental results

The proposed conf1 and conf2 sensor arrangements are analyzed on a single-inverter dual induction motor test stand. Both motors are mechanically coupled by a toothed belt drive that ensures synchronous rotation. Both motors have 13.8kW rated power.

Torque/flux estimation for conf1 and conf2

During following measurements, average rotor flux and average torque were controlled using the single torque and flux estimator of Fig. 2 and Fig. 3. The speed of both M1 and M2 is kept constant by a coupled machine. The speed is set to 30rpm.

In order to evaluate the control performance and torque/flux estimation, average rated flux is commanded. Average torque is varied stepwise. The results are shown in Fig. 4.

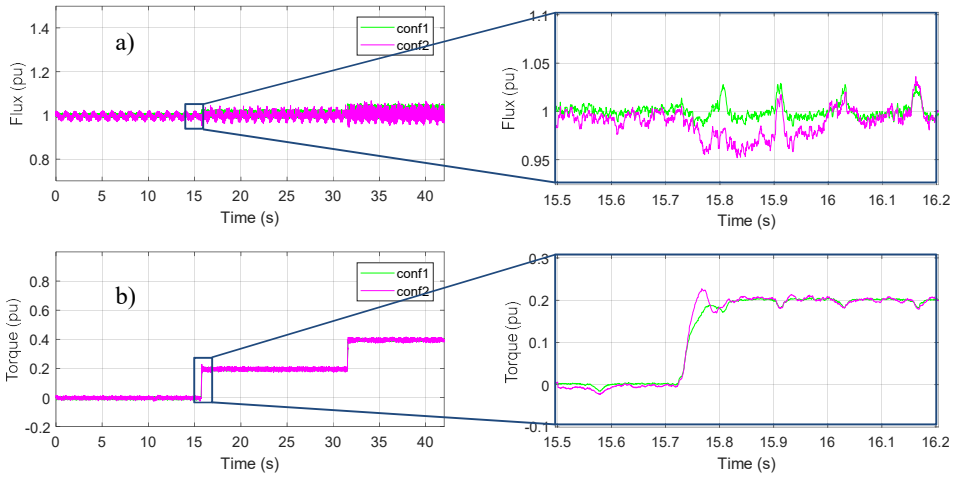

Fig. 4: conf1(green) and conf2 (magenta) flux and torque. a): average flux and zoom of it at 15.5s-16.2s. b): average torque and zoom of it at 15.5s-16.2s.

Regarding Fig. 4, it is worth noting that the torque and flux estimator in conf1 receives the stator sum current $\bar{\imath}_{S,M1+M2}^{(conf1)}$, which is actually being measured. However, conf2 needs to estimate $\bar{\imath}_{S,M2}^{(conf2)}$ in order to obtain the sum current. This explains the deviation from conf1 and conf2 torque and flux during transients (see Fig. 4). This implies that conf1 is more robust during transient operation than conf2. Yet, the transient characteristics of average flux and torque using conf2 strongly depend on the employed method to estimate $\bar{\imath}_{S,M2}^{(conf2)}$.

The M1 and M2 flux and torque are depicted in Fig. 5 using both configurations. Note that M1 conf2 torque and flux are magnitudes computed using the measured stator current vector of M1 (Fig. 5 a) and c)). For M2, both conf1 and conf2 stator currents are estimated using (26) and (31). Therefore, M2 “actual” torque and flux (additionally calculated using 2 current sensors on M2 A and B phases) are plotted together with the estimated conf1 and conf2 stator current vectors of M2.

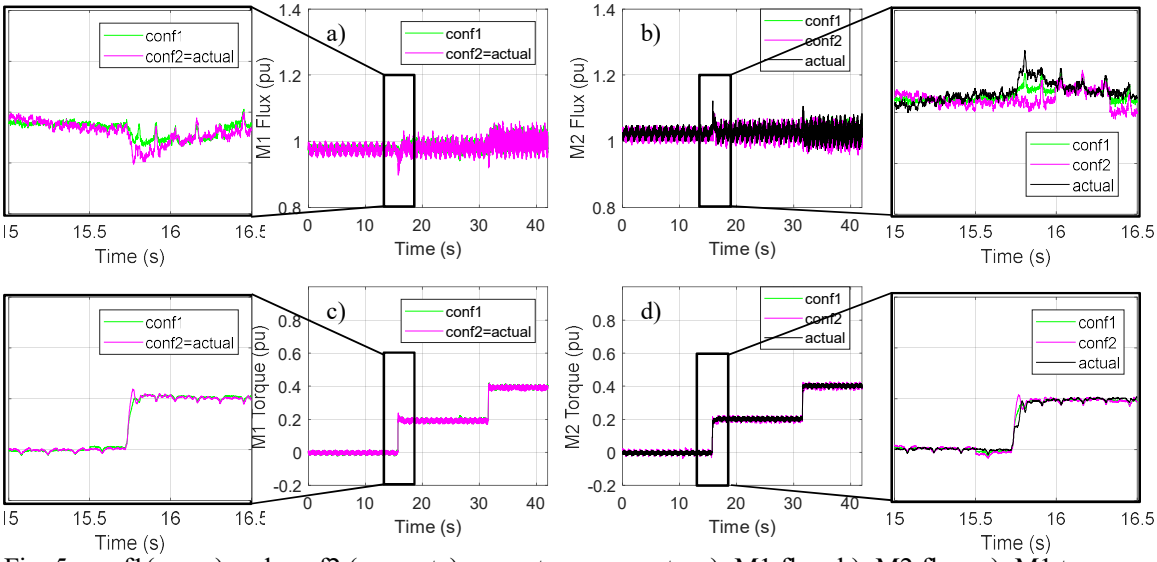

Fig. 5: conf1(green) and conf2 (magenta) current components. a): M1 flux. b): M2 flux. c): M1 torque. d): M2 torque.

As observed in Fig.5 b) and d), transient deviations in the M2 torque and flux are observed. This is due to the need for estimating the M2 stator current vector in both conf1 and conf2. Regarding M1, Fig.5 a) and c) show transient deviations in the M2 torque and flux for conf1. The M2 torque and flux estimator of conf2 uses the measured M2 stator current vector, thus representing the "actual" magnitudes.

Saliency amplitudes

For the two induction motors under test, multiple saliencies are present in the saliency vector $\bar{v}_{sal}$. In order to access rotor slotting, saturation and intermodulation (non-control saliencies) are identified using FFT. The offset present at $\bar{v}_{sal,M2}^{(conf2)}$, $\bar{v}_{sal,M1}^{(conf1)}$ and $\bar{v}_{sal,M1}^{(conf1)}$ is also identified.

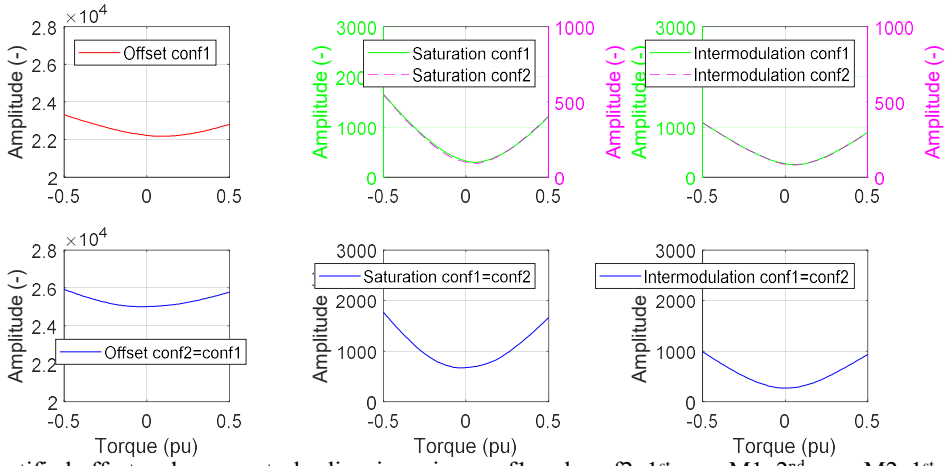

Fig. 6: Identified offset and non-control saliencies using conf1 and conf2. 1st row: M1. 2nd row: M2. 1st column: offset amplitude. 2nd column: saturation amplitude. 3rd column: intermodulation amplitude.

In order to access rotor slotting, offset and non-control saliencies are feed-forward compensated.

Encoderless operation

This subsection shows the saliency-offset vectors and encoderless operation for both motors and for both conf1 and conf2. During following measurement, the speed of both M1 and M2 is kept constant by a coupled machine at 20rpm. The dual motors are controlled at rated rotor flux and variable torque, varied from 20-50%. The resulting saliency-offset vector of each motor for each configuration is processed to deliver the slotting angle. It is achieved by means of feedforward compensating the offset (for the configurations where it is present) as well as the non-control saliencies. The results of the encoderless operation are shown in Fig. 7.

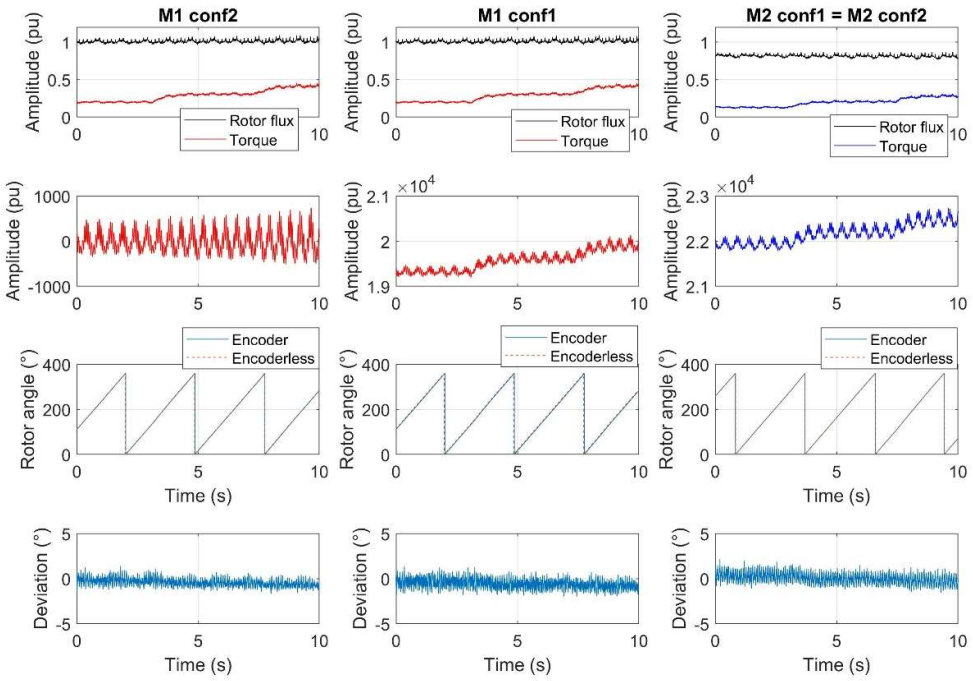

Fig. 7: Encoderless operation results for M1 conf2 (1st column), M1 conf1 (2nd column) and M2 (both conf1 and conf2, 3rd column). 1st row: rotor flux and torque. 2nd row: real part of saliency-offset vector. 3rd row: encoderless and shaft encoder angle. 4th row: deviation between encoderless and encoder angles.

As observed in Fig. 7, the saliency-offset vector of M1 for conf2 (2nd row 1st column) has zero offset due to the mathematical compensation as it was derived in (21). However, the saliency-offset vector of M1 for conf1 as well as that from M2 (for both conf1 and conf2) presents an offset. Both offset and non-control saliencies are feedforward compensated, thus only rotor slotting remains in the saliency vector. The angle of the slotting saliency is transformed into a rotor angle using the rotor slot number. The resulting encoderless angles are shown in Fig. 7, 3rd row. As the 4th row shows, very accurate rotor angles are obtained, having a maximum deviation of ±1.5° compared to the rotor angle measured by a shaft encoder. The angle deviation of M1 when conf2 is used is slightly smaller than when using conf1. This is due to the increased amount of current sensors in M1 for conf2.

Conclusion

Single-inverter dual induction motor drives commonly rely on four current sensors in total that are attached to two phases of each motor, thus permitting torque sharing calculation and individual spatial saliency extraction.

This work has investigated the use of two configurations (conf1, conf2) with reduced number of current sensors applied to a drive with two induction motors (M1, M2) connected in parallel and fed

by a single inverter. Both configurations consist of only three current sensors in total. In conf1, two current sensors are attached to two inverter output phases, and the remaining current sensor is attached to one phase of M2. In conf2, two current sensors are attached to two phases of M1, and the remaining current sensor is attached to one phase of M2. In order to extract motor saliencies, voltage step excitation is used. Besides, the control strategy is field-oriented control, where a single torque and flux estimator is implemented with the average stator current and average rotor angle as input.

Both current sensor configurations have been discussed and compared in terms of torque sharing capability, control performance and spatial saliency extraction. An experimental test stand equipped with two similar induction motors connected in parallel has been presented. The experimental measurements proved that a saliency-offset vector can be obtained when a single current sensor is attached to the motor, such as for M1 (conf1) and M2 (conf1 and conf2). To access saliencies, the offset was feedforward compensated. If two sensors are attached (M1, conf2), the offset can be mathematically eliminated and the saliency signal to noise ratio is increased, which leads to the acquisition of a slightly better rotor angle. Regarding torque sharing calculation, transient deviations in the rotor flux and torque were measured at M1 (conf1) and M2 (conf1 and conf2). This is because the torque and flux estimator employed for field-oriented control received an estimated averaged stator current phasor. In this sense, conf1 is more prone to transient deviations in torque sharing calculation. Experimental results on average torque and flux further suggested that conf1 has increased stability and robustness since the sum stator current is directly measured.

References

[1] E. Rodriguez Montero, M. Vogelsberger, M. Bazant, T. Wolbank, “Saliency-based Speed Sensorless Control of Single-Inverter Dual Induction Machines using Reduced Amount of Current Sensors”, *IEEE Energy Conversion Congress and Exposition (ECCE)*, pp. 5098-5103, 2020.

[2] E. Rodriguez Montero, M. Vogelsberger, M. Bazant, T. Wolbank, “A New Approach to Detect Load Sharing of Dual-Motors Driven and Controlled by a Single Converter using Only Three Current Sensors”, *IEEE International Conference on Electrical Machines (ICEM)*, pp.1040-1045, 2020.

[3] Y. Sua, M. Sumner, G. Asher, Q. Gao, K, Saleh, “Improved sensorless control of a permanent magnet machine using fundamental pulse width modulation excitation.” *IET Electric Power Application*, Vol. 5, pp. 359-370, Apr. 2011.

[4] M. X. Bui, D. Guan, D. Xiao, and M. Faz Rahman, “A modified sensorless control scheme for interior permanent magnet synchronous motor over zero to rated speed range using current derivative measurements,” *IEEE Trans. Ind. Electron., vol. 66, no. 1*, pp. 102–113, Jan. 2019.

[5] L. Guo, Z. Yang, F. Lin, and X. Tu, “Weighted torque current control for high speed train with dual induction motors fed by a single inverter,” in *Annual Conference of the IEEE Industrial Electronics Society*, pp. 2723–2728, Nov 2015.

[6] F. Xu, L. Shi, “Unbalanced thrust control of multiple induction motors for traction system”, in *IEEE Industrial Electronics and Applications Conference*, pp. 2752-2757, June 2011.

[7] F. Xu, L. Shi, and Y. Li, “The weighted vector control of speed-irrelevant dual induction motors fed by the single inverter,” *IEEE Trans. Power Electron.*, vol. 28, no. 12, pp. 5665–5672, Dec. 2013.

[8] T. I. Yeam, D. C. Lee, "Design of Sliding-Mode Speed Controller With Active Damping Control for Single-Inverter Dual-PMSM Drive Systems", in *IEEE Trans. on Power. Elect*., vol. 36, iss. 5, Mai 2021.

[9] Š. Janouš, J. Talla, V. Šmídl, Z. Peroutka, "Constrained LQR Control of Dual Induction Motor Single Inverter Drive", in *IEEE Trans. on Ind. Elect*., vol. 68, no. 7, pp. 5548-5558, July 2021.

[10] Q. Geng, Z. Li, M. Zhang, Z. Zhou, H. Wang, T. Shi, "Sensorless Control Method for Dual Permanent Magnet Synchronous Motors Driven by Five-Leg Voltage Source Inverter", in *IEEE Journal of Emerging and Selected Topics in Power Electronics*, June 2021.